Influence of Mesoporous Titanium Dioxide Layer on Perovskite Solar Cell Efficiency

Tanapornchai Lertkittimasak[1], Samuk Pimanpang[2], Pichet Limsuwan[1] and Witoon Yindeesuk[1,*]

[1] *Department of Physics, Faculty of Science, King Mongkut's Institute of Technology Ladkrabang, Bangkok, 10520, Thailand*

[2] *Department of Physics, Faculty of Science, Srinakharinwirot University, Bangkok, 10110, Thailand*

Received: 30 April 2022, Revised: 15 June 2022, Accepted: 27 June 2022

Abstract

This article studied mesoporous TiO_2 on the power conversion efficiency of perovskite solar cells by fabricating TiO_2 paste instead of prefabricated TiO_2, cutting the hole-transport layer, and using carbon instead of gold electrodes. The fabricated perovskite solar cells (PSCs) feature FTO glass/compact TiO_2/mesoporous TiO_2/$CH_3NH_3PbI_3$/carbon electrodes. The mesoporous TiO_2 layer was prepared from anatase TiO_2 and dissolved in ethanol at the ratios of 2.63, 1.27, 0.65, and 0.32%, respectively. The best perovskite solar cell efficiency was obtained using a mesoporous TiO_2 cell at a concentration of 1.27% with an open-circuit voltage (V_{oc}) of 0.41 V, short-circuit current density (J_{sc}) of 3.48 mA/cm^2, fill factor (FF) of 0.3, and power conversion efficiency (PCE) of 0.44%.

Keywords: Mesoporous titanium dioxide, Perovskite solar cell, Solar cell efficiency

1. Introduction

At present, there is a need for more electricity. The generated electricity can be exhausted as most of the electricity is generated from non-renewable energy such as natural gas, coal, petroleum, and other energies. Therefore, new backup power sources are being developed to replace the non-renewable energy sources to meet the demand for electricity in the future. Alternative energy sources should be domestically available, abundant, low production cost, and clean and sustainable. Considering all the above conditions, one of the answers to the energy problem is a solar energy source and solar cell technology. Single-junction silicon solar cells are mainly used, with the power conversion efficiency limited to 29.4% [1]. In the past few years, a type of solar cell has evolved by leaps and bounds, starting at 3.81% [2] to 25.2% [3] of perovskite solar cell.

Perovskite solar cell, the third generation of solar cells, is currently receiving much attention, and the power conversion efficiency is equivalent to silicon solar cell. Due to its simple production process, it does not require advanced technology for production. It has high absorbance, a high motion, and a diffusion distance coefficient, and the power conversion efficiency is equivalent to silicon solar cell [4]-[9]. However, the primary drawbacks of third-generation solar cells are their poor power conversion efficiency compared to inorganic solar cells and their long-term stability difficulties [10], [11]. The critical component used in manufacturing perovskite solar cells is methylammonium lead halide ($CH_3NH_3PbX_3$, X= Cl, Br, I) and halide crystals that correlate to perovskite's three-dimensional structure [11], [12]. The perovskite solar cell is composed of three major components:

Corresponding Author : witoon.yi@kmitl.ac.th

1) The anode electrode consists of a perovskite compound coated on metal oxide thin film on the glass.
2) The hole carrier transports the hole from the perovskite compound to the cathode electrode.
3) The cathode electrode collects the hole or positive charge.

A perovskite solar cell typically consists of a conductive substrate, electron transport layer (ETL), perovskite light-absorbing layer, hole transport layer, and electrodes. The electron transport layer plays a vital role in charge carrier and electron dissociation. TiO_2 is utilized to form an electron transport layer, which serves as electron transport and hole blocking. Titanium dioxide is widely used in solar cell construction due to its wide bandgap, high transparency, high electron mobility, suitable transmission band, and low cost [13]-[16]. Titanium dioxide exhibits poor optical scattering properties in the visible light region due to the small size of TiO_2 nanoparticles, resulting in low-light harvesting efficiency. Several researchers have shown that these problems can be improved by modifying the structure of the electron transport layer to achieve better solar cell performance. Introducing some interface-modified materials allows for more uniform perovskite film leading to a more functional perovskite absorbance layer. The electron transport layer is a mesoporous TiO_2 structure that provides high power conversion efficiency [17]-[19] due to improved film morphology, light absorption, light scattering, improved conductivity, and decreased recombination. The electron transport structure consists of a compact TiO_2 layer, a mesoporous TiO_2 layer, and is coated with perovskite, a solar absorber. A high-temperature annealing process is typically employed for fabricating the electron transport layer [17]-[20].

Nevertheless, cell production in some structures is also costly and complicated. Therefore, the hole transport material structures (HTMs) that act as electron-blocking layers and stabilize devices was avoided, such as spiro-OMeTAD [12], 2poly[*bis*(4-phenyl)(2,4,)6-trimethylphenyl)amine] (PTAA) [21], and poly(3-hexylthiophene-2,5-diyl) (P3HT) [22]. Carbon as a counter electrode (CE) used instead of metal has families such as Au or Ag to reduce the cost of perovskite solar cells production [23]-[27].

In this paper, Perovskite solar cell fabrication using TiO_2 with a mesoporous electron transport layer was fabricated from anatase TiO_2 [28] to achieve improved efficiency of perovskite solar cells satisfying and reducing the hassle of producing cells. Structure of perovskite solar cells is FTO/compact TiO_2/mesoporous TiO_2/$CH_3NH_3PbI_3$/carbon electrode. For the compact TiO_2 layer, we will use a total of 2 concentrations of TiO_x since the influence of TiO_{x1}, and TiO_{x2} affects the compact TiO_2 layer in terms of film thickness and surface coverage of the FTO glass across the sheet. It will not cause leakage at the TiO_2 layer; any leakage will cause the cell to have a low voltage difference or an electric shock circuit. The cell structure is HTM-free, and carbon paste was used to develop the electrode instead of Au or Ag. Carbon was deposited onto the perovskite layer by the doctor blade technique.

2. Experimental

2.1 Materials

All the chemical materials are laboratory-grade including titanium diisopropoxide *bis*(acetylacetonate) 75 wt. % in isopropanol and Lead(ll) iodide 99% purchased from ALDRICH Chemistry. Methylammonium iodide >99.99% (MAI) was purchased from Greatcell Solar Materials. Acetylacetone ReagentPlus®, ≥99% (2,4-Pentanedione), *N*, *N*-dimethylformamide anhydrous 99.8% (DMF), Dimethyl sulfoxide anhydrous ≥99.9% (DMSO), 2-Propanal anhydrous 99.5% and chlorobenzene anhydrous 99.8% were purchased

from SIGMA-ALDRICH. Titanium dioxide nanopowder (TiO_2 anatase, 99.5%, 15 nm) was purchased from US Research Nanomaterials and polyethylene glycol 500,000 was purchased from FUJIFILM Wako Pure Chemical Corporation.

2.2 Mesoporous TiO_2 preparation

Mesoporous TiO_2 was prepared by stirring 3 g of titanium dioxide nanopowder (TiO_2 anatase, 99.5%, 15 nm) and 1.2 g of polyethylene glycol 500,000 (PEG) in 10 mL of DI water and 1 mL of acetylacetone for 1 h. The resulting paste was mixed with ethanol at the ratios of 2.63, 1.27, 0.65, and 0.32 wt%, respectively then stirred at 80°C for 1 h.

2.3 Preparation of perovskite solar cell

The substrates used in this work were FTO glasses, each with a 20 mm x 20 mm. Etching glass used zinc powder mixed with DI water, and a drop of HCl acid was applied to remove the electrodes. The glass was cleaned with an ultrasonic cleaner four times and each time for 15 min. The solutions used for cleaning were: (1) water with detergent, (2) water, (3) DI water, and (4) ethanol, respectively. The clean substrates were dried for about 10 min. The concentration of TiO_{x1} was prepared from 20 0 µL titanium diisopropoxide, and 2.520 mL IPA (2-propanol), whereas TiO_{x2} was prepared from 20 0 µL titanium diisopropoxide and 1.160 mL IPA (2-propanol). The 60 µL of TiO_{x1} solution was dropped on the glass surface area to be coated, and the spin coating was performed at 3000 rpm for 45 s. Then, it was annealed on a hot plate at 120°C for 10 min then cooled down. Spin coating was repeated by using TiO_{x2} compound solution. After coating, the sample was annealed at 500°C for 1 h. Each concentration of mesoporous TiO_2 was then coated on top of the previous film by the spin coating method. The coated glass was dropped with 50 µL of mesoporous TiO_2 and was spun at 4000 rpm for 45 s. Then, it was dried on a hot plate at 80°C for 10 min. After, the glass was dried and heated at 500°C for 1 h. Perovskite was produced from 0.1589 g methylammonium iodide (MAI) and 0.4610 g lead (II) iodide (PbI_2). The powder was dissolved with solvent N, N -dimethylformamide (DMF), and dimethyl sulfoxide (DMSO) (volume ratio 9:1 Perovskite layer coating starts by heating the prepared glass with a hot plate at 145°C for 2 min. Then, the glass was put into a spin coater, dropping 60 µL of $MAPbI_3$, and the spin coating was performed at 3000 rpm for 45 s. About 10 s before completing spin coating, 150 µl chlorobenzene was gently dropped onto the film surface. Then, it was dried on a hot plate at 125°C for 20 min. After the film was dried, the electrodes were constructed from carbon paste by the doctor blade method and dried on a hot plate at 100°C for 10 min.

2.4 Characterization methods

The XRD pattern of anatase TiO_2 was obtained using X-ray diffraction (XRD). The transmittance and light absorption of TiO_2 was measured by a UV 2600 UV-Vis spectrophotometer in the 200-1400 nm wavelength. The solar simulator was employed to measure current-voltage characteristics (I-V) and power conversion efficiency of a perovskite solar cell with a 150 W short-arc Xe lamp light source. The photovoltaic properties were evaluated under 100 mW/cm^2 (1.0 sun) and higher (A.M. 1.5G, Effective illumination area). Cross-section and surface morphology of the TiO_2 samples was studied using FEI QUANTA 250 scanning electron microscopy (SEM).

3. Results and discussion

XRD patterns of the stirring-prepared mesoporous TiO_2 are shown in Fig. 1. The synthesized mesoporous TiO_2 characterizes crystals with laying 2θ peaks at 25.26° (101), 37.84° (004), 48° (200), 53.94° (105), and 62.66° (204). All peaks obtained from the XRD

model, TiO_2 anatase phase, and diffraction data are consistent with Vijayalakshmi *et al.* [29]. The crystal size was calculated from the formula of Debye-Scherrer given by the equation (1).

$$D = \frac{0.9\lambda}{\beta\cos\theta} \quad (1)$$

D is the crystal size, λ is the X-ray wavelength (λ=0.15406 nm), and β is the line width at half the maximum peak. The calculated crystal size of mesoporous TiO_2 is approximately 19 nm.

Fig. 2 shows the UV-vis light transmission spectra of mesoporous TiO_2 at different concentrations. Mesoporous TiO_2 at concentration 1.27 wt% has the superior light transmittance suited to mesoporous layers that require as much light to penetrate the perovskite layer as possible.

Fig. 3 shows UV-vis absorbance spectra of mesoporous TiO_2 films produced with various TiO_2 paste concentrations. The mesoporous TiO_2 film shows the peak of the absorbance of each concentration at about 310-320 nm and does not indicate a strong absorbance over the 400-1400 nm region. Therefore, the mesoporous TiO_2 layer is transparent in the 400-1,400 nm range.

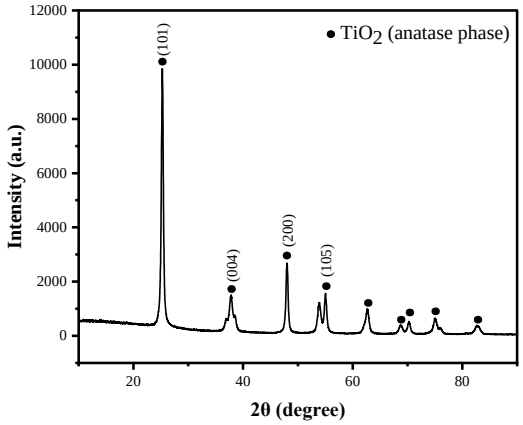

Fig. 1. XRD patterns of mesoporous TiO_2 synthesized via the stirring method

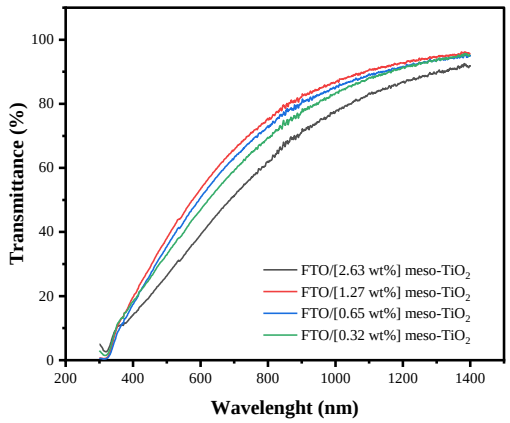

Fig. 2. UV–vis transmission spectra of mesoporous TiO_2 concentration deposited on FTO glass by spin coating

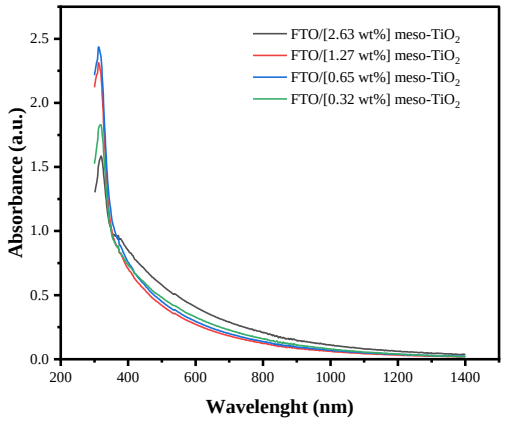

Fig. 3. UV–vis absorbance spectra of mesoporous TiO_2 concentration deposited on FTO glass by spin coating

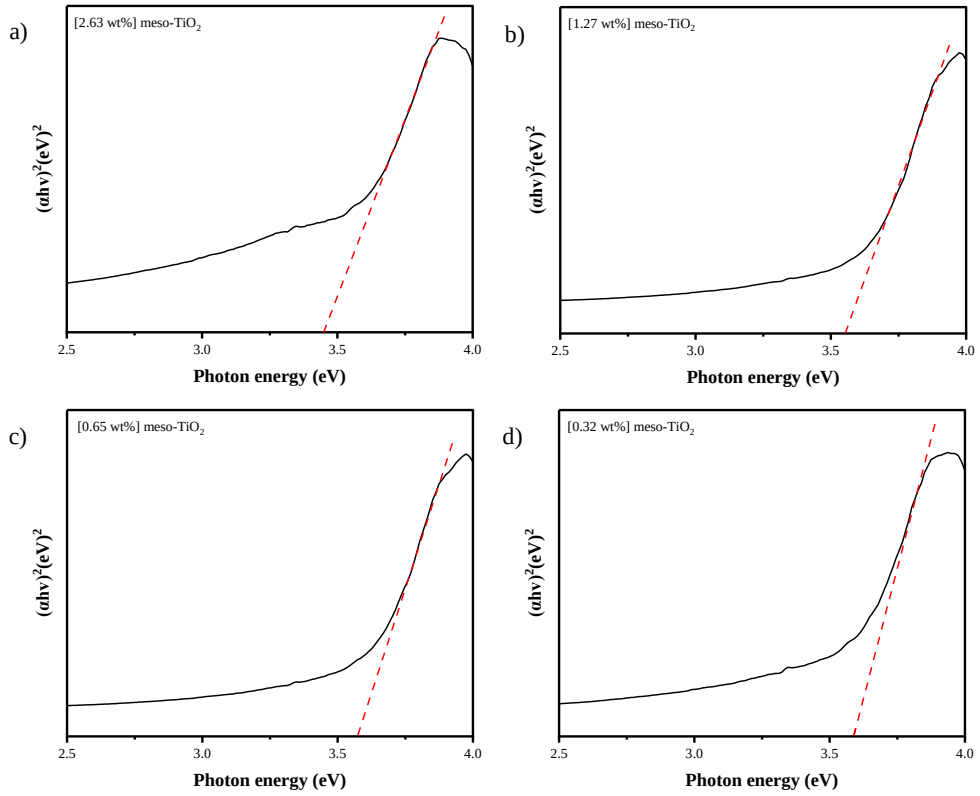

Fig. 4. Tauc plot and corresponding bandgap of (a) [2.63 wt%] meso-TiO_2, (b) [1.27 wt%] meso-TiO_2, (c) [0.65 wt%] meso-TiO_2, and (d) [0.32 wt%] meso-TiO_2

Fig. 4 shows the Tauc plot and bandgaps of the samples with different concentrations of mesoporous TiO_2 (2.63, 1.27, 0.65, and 0.32 wt%) films. The mesoporous TiO_2 band gap was calculated using the Tauc plot relationship expressed by equation (2).

$$\alpha = \frac{A(h\nu - Eg)^n}{h\nu} \quad (2)$$

Where E_g is the absorption bandgap, α is the absorption coefficient, A is a constant, and n may have direct, indirect, forbidden direct, and forbidden indirect transitions that are represented by the values 1/2, 2, 3/2, and 3, respectively. In this research, n=1/2 is used for direct transition. In addition, Table 1 also indicates the bandgap estimated from the Tauc plot drawn using the UV-vis spectrum. Among all samples, [0.65 wt%] meso-TiO_2 sample possesses the greatest bandgap of 3.57 eV. As the concentration of mesoporous TiO_2 declines, the band gap expands with a decrease in the particle size, and the absorption edge shifts to higher energy (blue shift).

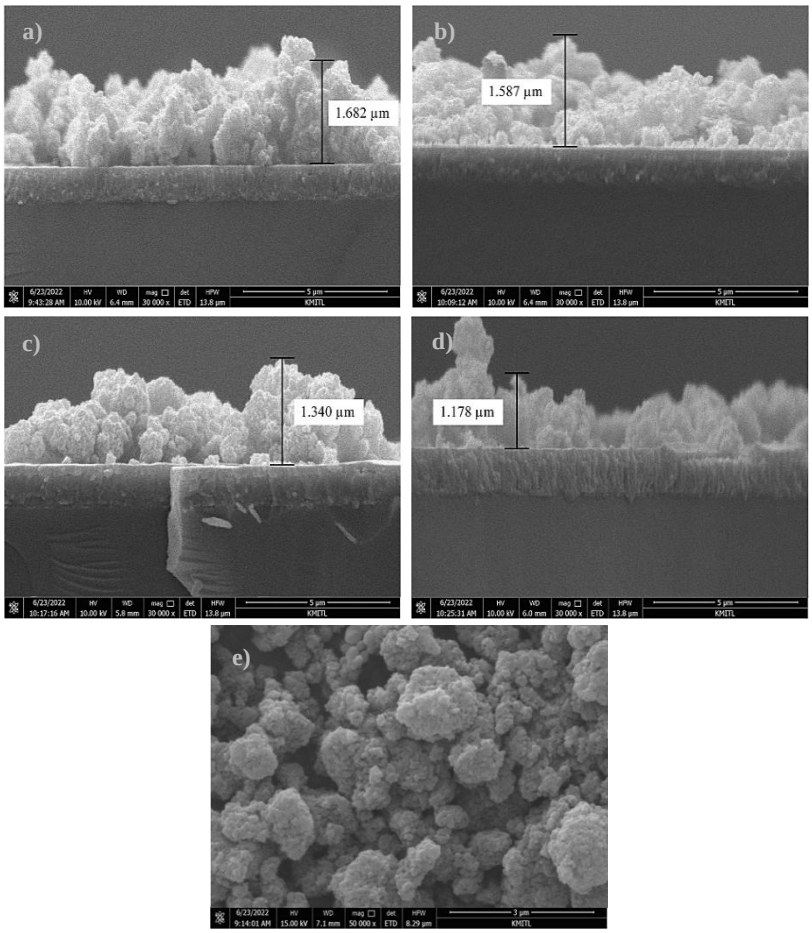

Fig. 5. SEM images of mesoporous TiO_2 devices in cross-sectional and SEM images on the surface morphology of mesoporous TiO_2 films: a) [2.63 wt%] meso-TiO_2 yielded a TiO_2 film thickness of 1.682 µm, b) [1.27 wt%] meso-TiO_2 yielded a TiO_2 film thickness of 1.587 µm, c) [0.65 wt%] meso-TiO_2 yielded a TiO_2 film thickness of 1.340 µm, d) [0.32 wt%] meso-TiO_2 yielded a TiO_2 film thickness of 1.178 µm, and e) SEM micrograph of mesoporous TiO_2 at a concentration of 1.27 wt%

Fig. 5 a)-d) show SEM images of a cross-sectional film thickness of the samples with various TiO_2 concentrations. It is revealed that high TiO_2 concentrations resulted in a highly thick mesoporous TiO_2 layer and a lower light transmission rate to the perovskite layer resulted in low efficiency. The lower the TiO_2 concentration, the thinner the film created, the better the light transmittance, and the higher the efficiency. The optimal concentration for optimizing light transmission from the TiO_2 layer to the perovskite layer is 1.27wt %,

Table 1. The energy bandgap (E_g) of concentration TiO_2 from Tauc plot

Sample	E_g [eV]
[2.63 wt%] meso-TiO_2	3.45
[1.27 wt%] meso-TiO_2	3.54
[0.65 wt%] meso-TiO_2	3.57
[0.32 wt%] meso-TiO_2	3.54

resulting in a TiO_2 layer thickness of 1.587 µm. The SEM image (Fig. 5 e)) shows the TiO_2 film surface morphology at a concentration of 1.27 wt%, which results in the highest power conversion efficiency and could confirm that the TiO_2 applied in the electron transport layer was mesoporous TiO_2.

Fabrication of Perovskite solar cells is in N-I-P structures following FTO glass/compact TiO_2/mesoporous TiO_2/$CH_3NH_3PbI_3$/carbon electrode with mesoporous TiO_2 concentrations of 2.63, 1.27, 0.65, and 0.32 wt%. The cell structure is HTM-free, and carbon paste was used to develop the electrode. The doctor blade technique was used to deposit carbon onto the perovskite layer. Fig. 6 shows the structure of a solar cell. The power conversion efficiency (PCE), which indicates the efficiency of photovoltaic devices, was calculated using equation (3).

$$\eta = \frac{\text{Voc Jsc FF}}{\text{Pin}} \tag{3}$$

Where J_{sc} indicates the short-circuit current density, V_{oc} indicates open-circuit voltage, FF indicates fill-factor, P_{in} power of incident light of 100 W/cm^2, and η is the power conversion efficiency. The equation (4) can be used to determine FF, where V_{mp} is the maximum voltage, and J_{mp} is the maximum current.

$$\text{FF} = \frac{\text{Vmp Jmp}}{\text{Voc Jsc}} \tag{4}$$

Fig. 7 shows the photocurrent-voltage (IV) characteristic of a perovskite solar cell, indicating that a mesoporous TiO_2 concentration of 1.27 wt% gives a higher current density than other mesoporous TiO_2 concentrations.

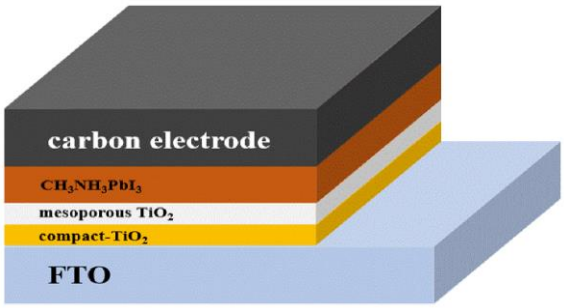

Fig. 6. Schematic representation of the fabricated Perovskite solar cell structure

Fig. 8 shows the resulting efficiency of perovskite solar cells as determined by using a solar simulator under one sun of 100 mW/cm^2. Each Perovskite solar cell is in an active area of 0.5 cm^2. The best and average photovoltaic data of 10 samples with different mesoporous TiO_2 concentrations are given in Table 2.

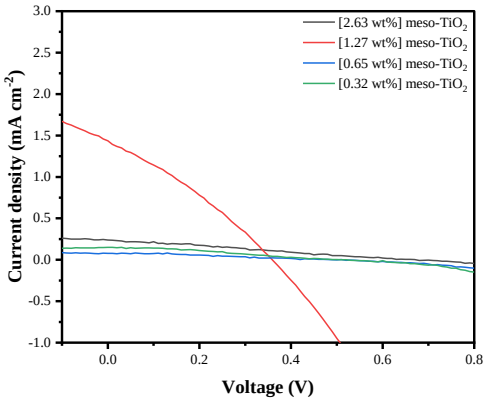

Fig. 7. A perovskite solar cell without a mesoporous TiO_2 and with mesoporous TiO_2 concentrations of 2.63, 1.27, 0.65, and 0.32 wt %

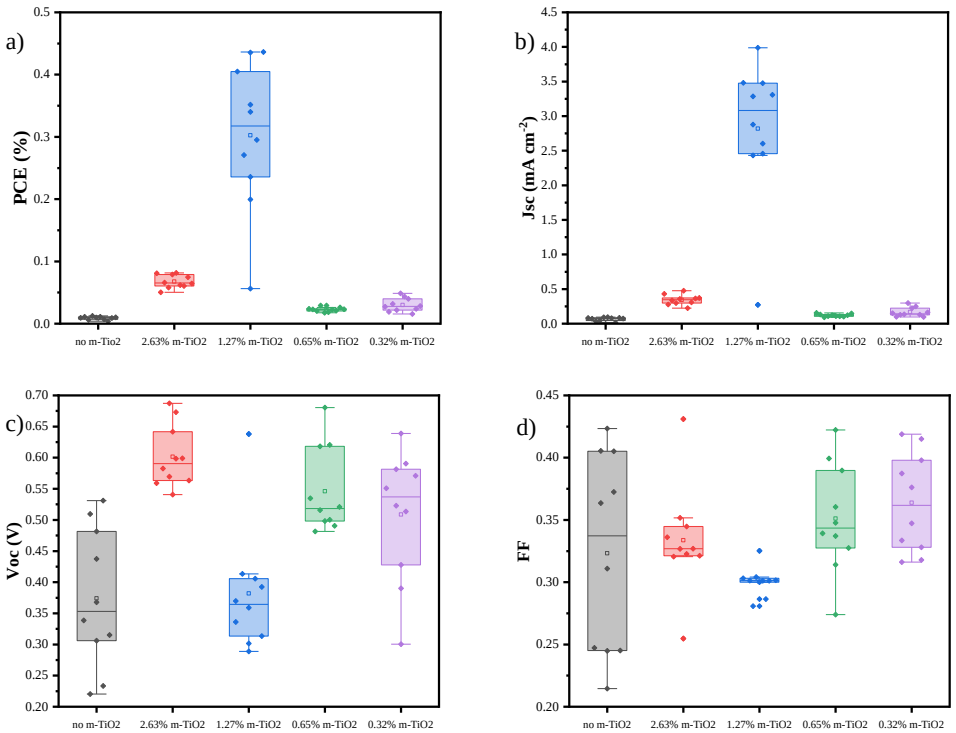

Fig. 8. The variations in a) *PCE*, b) J_{sc}, C) V_{oc}, and d) *FF* of various perovskite solar cells fabricated using different mesoporous TiO_2 of 10 samples for each concentration

Table 2. Photovoltaic parameters of FTO/compact, TiO_2/mesoporous, TiO_2/$CH_3NH_3PbI_3$/carbon electrode with an active area of 0.5 cm^2 fabricated by mesoporous TiO_2 with different concentrations

Sample	J_{sc} [mA/cm^2]	V_{oc} [V]	FF	PCE [%]
No meso-TiO_2				
Average	0.06	0.37	0.32	0.01
Best PCE	0.04	0.53	0.42	0.01
[2.63 wt%]meso-TiO_2				
Average	0.34	0.60	0.33	0.07
Best PCE	0.48	0.67	0.25	0.08
[1.27 wt%]meso-TiO_2				
Average	2.82	0.38	0.30	0.30
Best PCE	3.48	0.41	0.30	0.44
[0.65 wt%]meso-TiO_2				
Average	0.12	0.55	0.35	0.02
Best PCE	0.11	0.68	0.39	0.03
[0.32 wt%]meso-TiO_2				
Average	0.17	0.51	0.36	0.03
Best PCE	0.30	0.51	0.32	0.05

Compared to other mesoporous TiO_2 concentrations, perovskite solar cells with a 1.27 wt % mesoporous TiO_2 concentration applied as a mesoporous TiO_2 layer showed the best power conversion efficiency and current density compared to other mesoporous TiO_2 concentrations. It can achieve short-circuit current density (J_{sc}) of 3.48 mA/cm^2, open-circuit voltage (V_{oc}) of 0.41 V, fill factor (*FF*) of 0.3, and power conversion efficiency (*PCE*) of 0.44%. However, the power conversion efficiency effect of our work is unsatisfactory compared to other works such as Zheng *et al.* [26] used mesoporous TiO_2 (OPV-18NR-T) as an electron transport layer which can provide efficiency up to 8.45%, Etgar *et al.* [30] brought TiO_2 nanosheets used to transport electrons showed power conversion efficiency of 7.3%, and Zhang *et al.* [31] used TiO_2 paste (18NR-T Dyesol) as the electron transport layer which showed the best power conversion efficiency of 8.31%. Our work's energy transformation efficiency is inadequate because our mesoporous TiO_2 has low charge recombination, which is insufficient. The open-circuit voltage is 0.41 V, indicating this. For future work, it is also recommended that the power conversion efficiency of perovskite solar cells be improved by modifying the structure of the blocking layer TiO_2 or adding a compound that reduces charge recombination [32], [33].

4. Conclusion

Different mesoporous TiO_2 concentrations affect light transmittance differently. These are among the parameters affecting the efficiency of perovskite solar cells. The less incident light on the active or perovskite layer could reduce power conversion efficiency. The optimal mesoporous TiO_2 concentration for this work was 1.27 wt%, the concentration at which light transmittance in the visible light spectrum was greatest and with the energy bandgap of 3.54 eV. The best achievable power conversion efficiency is 0.44%. However, other mesoporous TiO_2 concentrations resulted in descending conversion efficiency: mesoporous TiO_2 concentrations of 2.67, 0.32, and 0.65 wt%, yielding power conversion efficiency of 0.08%, 0.05%, and 0.03%, respectively. The film yielding the least power conversion efficiency was

the uncoated film with a mesoporous TiO_2 which yields the power conversion efficiency of 0.01%.

Acknowledgement

The Faculty of Science of King Mongkut's Institute of Technology Ladkrabang and the Faculty of Science of Srinakharinwirot University received support for this research.

References

[1] Richter A, Hermle M, Glunz SW. Reassessment of the limiting efficiency for crystalline silicon solar cells. IEEE J. Photovoltaics 2013;3(4):1184-91.
[2] Kojima A, Teshima K, Shirai Y, Miyasaka T. Organometal halide perovskites as visible-light sensitizers for photovoltaic cells. J. Am. Chem. Soc. 2009;131(17):6050-1.
[3] US National Renewable Energy Laboratory. Catalysis from A to Z. 2020.
[4] Dennler G, Scharber MC, Brabec CJ. Polymer-fullerene bulk-heterojunction solar cells. Adv. Mater. 2009;21(13):1323-38.
[5] Stranks SD, Eperon GE, Grancini G, Menelaou C, Alcocer MJP, Leijtens T, *et al.* Electron-hole diffusion lengths exceeding 1 micrometer in an organometal trihalide perovskite absorber. Science 2013;342(6156):341-4.
[6] Green MA, Ho-Baillie A, Snaith HJ. The emergence of perovskite solar cells. Nat. Photonics 2014;8(7):506-14.
[7] Wehrenfennig C, Eperon GE, Johnston MB, Snaith HJ, Herz LM. High charge carrier mobilities and lifetimes in organolead trihalide perovskites. Adv. Mater. 2014;26(10): 1584-9.
[8] Fan J, Jia B, Gu M. Perovskite-based low-cost and high-efficiency hybrid halide solar cells. Photonics Res. 2014;2(5):111-20.
[9] Shi D, Adinolfi V, Comin R, Yuan M, Alarousu E, Buin A, *et al.* Low trap-state density and long carrier diffusion in organolead trihalide perovskite single crystals. Science 2015;347(6221):519-22.
[10] Nelson J. Organic photovoltaic films.Curr. Opin. Solid State Mater. Sci. 2002;6:87-95.
[11] Lee MM, Teuscher J, Miyasaka T, Murakami TN, Snaith HJ. Efficient hybrid solar cells based on meso-superstructured organometal halide perovskites. science.2012;338 (6107):643-7.
[12] Kim HS, Lee CR, Im JH, Lee KB, Moehl T, Marchioro A, *et al.* Lead iodide perovskite sensitized all-solid-state submicron thin film mesoscopic solar cell with efficiency exceeding 9%. Sci. Rep. 2012;2:1-7.
[13] Liao HC, Lee CH, Ho YC, Jao MH, Tsai CM, Chuang CM, *et al.* Diketopyrrolopyrrole-based oligomer modified TiO_2 nanorods for air-stable and all solution processed poly(3-hexylthiophene):TiO_2 bulk heterojunction inverted solar cell. J. Mater. Chem. 2012; 22(21):10589-96.
[14] Aharon S, Gamliel S, Cohen B El, Etgar L. Depletion region effect of highly efficient hole conductor free $CH_3NH_3PbI_3$ perovskite solar cells. Phys. Chem. Chem. Phys. 2014; 16(22):10512-8.
[15] Tavakoli MM, Yadav P, Tavakoli R, Kong J. Surface engineering of TiO_2 ETL for highly efficient and hysteresis-less planar perovskite solar cell (21.4%) with enhanced open-circuit voltage and stability. Adv. Energy Mater. 2018;8(23):1-9.
[16] Kırbıyık Ç, Can M, Kuş M. Interfacial modification via boronic acid functionalized self-assembled monolayers for efficient inverted polymer solar cells. Mater. Sci. Semicond. Process. 2020;107:104860.

[17] Correa-Baena JP, Anaya M, Lozano G, Tress W, Domanski K, Saliba M, *et al.* Unbroken perovskite: Interplay of morphology, electro-optical properties, and ionic movement. Adv. Mater. 2016;28(25):5031-7.
[18] Saliba M, Matsui T, Seo JY, Domanski K, Correa-Baena JP, Nazeeruddin MK, *et al.* Cesium-containing triple cation perovskite solar cells: Improved stability, reproducibility and high efficiency. Energy Environ. Sci. 2016;9(6):1989-97.
[19] Noori L, Hoseinpour V, Shariatinia Z. Optimization of TiO_2 paste concentration employed as electron transport layers in fully ambient air processed perovskite solar cells with a low-cost architecture. Ceram. Int. 2022;48(1):320-36.
[20] Burschka J, Pellet N, Moon SJ, Humphry-Baker R, Gao P, Nazeeruddin MK, *et al.* Sequential deposition as a route to high-performance perovskite-sensitized solar cells. Nature 2013;499(7458):316-9.
[21] Heo JH, Im SH, Noh JH, Mandal TN, Lim CS, Chang JA, *et al.* Efficient inorganic-organic hybrid heterojunction solar cells containing perovskite compound and polymeric hole conductors. Nat. Photonics 2013;7(6):486-91.
[22] Wang H, Liu G, Li X, Xiang P, Ku Z, Rong Y, *et al.* Highly efficient poly(3-hexylthiophene) based monolithic dye-sensitized solar cells with carbon counter electrode. Energy Environ. Sci. 2011;4(6):2025-9.
[23] Wei H, Xiao J, Yang Y, Lv S, Shi J, Xu X, *et al.* Free-standing flexible carbon electrode for highly efficient hole-conductor-free perovskite solar cells. Carbon 2015;93:861-8.
[24] Maniarasu S, Korukonda TB, Manjunath V, Ramasamy E, Ramesh M, Veerappan G. Recent advancement in metal cathode and hole-conductor-free perovskite solar cells for low-cost and high stability: A route towards commercialization. Renewable Sustainable Energy Rev. 2018;82:845-57.
[25] Zhang Y, Zhang H, Zhang X, Wei L, Zhang B, Sun Y, *et al.* Major impediment to highly efficient, stable and low-cost perovskite solar cells. Metals 2018;8(11):1-33.
[26] Zheng H, Li C, Wei A, Liu J, Zhao Y, Xiao Z. Study of carbon-based hole-conductor-free perovskite solar cells. Int. J. Hydrogen Energy 2018;43(24):11403-10.
[27] Fagiolari L, Bella F. Carbon-based materials for stable, cheaper and large-scale processable perovskite solar cells. Energy Environ. Sci. 2019;12(12):3437-72.
[28] Shen Q, Toyoda T. Studies of optical absorption and electron transport in nanocrystalline TiO_2 electrodes. Thin Solid Films 2003;438-439(03):167-70.
[29] Vijayalakshmi R, Rajendran V. Synthesis and characterization of nano-TiO_2 via different methods. Sch Res Libr. 2012;4(2):1183-90.
[30] Etgar L, Gao P, Xue Z, Peng Q, Chandiran AK, Liu B, *et al.* Mesoscopic $CH_3NH_3PbI_3$/TiO_2 heterojunction solar cells. J. Am. Chem. Soc. 2012;134(42):17396-9.
[31] Zhang F, Yang X, Wang H, Cheng M, Zhao J, Sun L. Structure engineering of hole-conductor free perovskite-based solar cells with low-temperature-processed commercial carbon paste as cathode. ACS Appl. Mater. Interfaces 2014;6(18):16140-6.
[32] Liu G, Yang B, Chen H, Zhao Y, Xie H, Yuan Y, et al. In situ surface modification of TiO_2 by $CaTiO_3$ to improve the UV stability and power conversion efficiency of perovskite solar cells. Appl. Phys. Lett. 2019;115(21).
[33] Li T, Rui Y, Zhang X, Shi J, Wang X, Wang Y, et al. Anatase TiO_2 nanorod arrays as high-performance electron transport layers for perovskite solar cells. J. Alloys Compd. 2020;849:156629.